Front. Optoelectron. 2021, 14(4): 499–506
https://doi.org/10.1007/s12200-020-1103-2

RESEARCH ARTICLE

Light-emission organic solar cells with MoO_3:Al interfacial layer–preparation and characterizations

Xinran LI[1], Yanhui LOU (✉)[1], Zhaokui WANG (✉)[2]

1 College of Energy, Key Laboratory of Advanced Carbon Materials and Wearable Energy Technologies of Jiangsu Province, Soochow University, Suzhou 215006, China
2 Institute of Functional Nano & Soft Materials (FUNSOM), Soochow University, Suzhou 215123, China

Abstract A light-emitting organic solar cell (LE-OSC) with electroluminescence (EL) and photovoltaic (PV) properties is successfully fabricated by connecting the EL and PV units using a MoO_3:Al co-evaporation interfacial layer, which has suitable work function and good transmittance. PV and EL units are fabricated based on poly(3-hexylthiophene) (P3HT)-indene-C_{60} bisadduct ($IC_{60}BA$) blends, and 4,4′-bis (N-carbazolyl) biphenyl-fac-tris (2-phenylpyridine) iridium ($Ir(ppy)_3$), respectively. The work function and the transmittance of the MoO_3:Al co-evaporation are measured and adjusted by the ultraviolet photoelectron spectroscopy and the optical spectrophotometer to obtain the better bi-functional device performance. The forward- and reverse-biased current density-voltage characteristics in dark and under illumination are evaluated to better understand the operational mechanism of the LE-OSCs. A maximum luminance of 1550 cd/m^2 under forward bias and a power conversion efficiency of 0.24% under illumination (100 mW/cm^2) are achieved in optimized LE-OSCs. The proposed device structure is expected to provide valuable information in the film conditions for understanding the polymer blends internal conditions and meliorating the film qualities.

Keywords organic solar cell (OSC), polymer-fullerene, light emission, MoO_3:Al interfacial layer

1 Introduction

Conjugated polymers blended with soluble fullerene derivatives have demonstrated a remarkable potential for low-cost, large-area and flexible organic solar cells (OSCs) with exceeding 10% in power conversion efficiency [1]. For commercialization, further improvement in power conversion efficiency and the cell reliability are desired [2,3]. To the power conversion efficiency, there still exists the room of improvement by synthesizing more efficient materials [4], optimizing more rational device structure [5] and even electrical doping for improving the light-harvesting efficiency in polymer solar cells [6,7]. Importantly, the issue of cell stability has to be paid more attentions after the power conversion efficiency approaching 10%. There are many degradation channels during cell operation and each contributes to the overall deterioration of photovoltaic (PV) performance that consequently shortens the device lifetime. Great efforts have been taken in the cell stability especially the materials stability in OSCs. According to each layer that usually constitutes an OSC, the materials stability can be subdivided: active layer [8,9], electrodes [10,11], electron transport layer [12,13], and hole transport layer [14,15] which contributes their own degradation mechanisms. In addition, the physical stabilities such as the cell structure [16], the interfacial condition [17,18], and even the film processing means also play important roles in the whole cell degradation [19]. The most significant contributor is believed to be a combined effect by above mentioned mechanisms due to the diffusion of atmosphere species into the cells. Electrical trap states, which are mainly induced by the impurities and the structural defects in the organic bulk films [20,21], can be easily evaluated by basis electrical and/or optical measurements [22–25].

Electroluminescence (EL) imaging has been widely used as a photographic evaluation technique to indicate the cell physical properties in silicon solar cells [26–29]. The same function of EL imaging is also desired in OSCs, which is expected to provide valuable information on the film defects for meliorating the film quality and improving the device performance. Recently, Cravino et al. reported a

Received September 10, 2020; accepted November 1, 2020

E-mails: yhlou@suda.edu.cn (Y. Lou), zkwang@suda.edu.cn (Z. Wang)

light-emitting OSC (LE-OSC) based on a conjugated system with internal charge transfer [30]. Hoyer et al. demonstrated a weak EL imaging in polymer-fullerene based OSCs [31]. Tvingstedt et al. observed the EL phenomenon from several types of organic polymer-fullerene bulk heterojunction solar cells [32]. The general understanding treats light and current generations as competing process due to their reverse generation mechanism, which leads to very weak EL intensity in past reports. The EL intensity needs to be improved as high enough for clearly observing the microstructure of organic films. Other than inorganic based EL devices, noticeably, organic light-emitting device (OLED) is an innate surface-emitting light source, which makes it very appropriate to evaluate the film quality especially the film uniformity as a back light illumination. We try to observe the film quality of polymer-fullerene blends by using OLED as the back light illumination. It can be realized by connecting the PV unit and EL unit via an appropriate intermediate layer, which generally functions as an internal electrode to produce charge carrier and to facilitate the carriers into the adjacent units.

Poly(3-hexylthiophene) (P3HT) and indene-C_{60} bisadduct ($IC_{60}BA$) is the most intensely investigated conjugated polymer donor material and acceptor material, respectively. 4,4′-bis (N-carbazolyl) biphenyl (CBP)/fac-tris (2-phenylpyridine) iridium ($Ir(ppy)_3$) is a typical host/dopant system in OLEDs. In this paper, we demonstrate a bi-functional LE-OSC by connecting separated PV unit (P3HT:$IC_{60}BA$ as the active layer) and EL unit (CBP:$Ir(ppy)_3$ as the emitting layer) using a MoO_3:Al co-deposited interfacial layer. The work function and the transmittance of the MoO_3:Al co-evaporation are measured and adjusted by the ultraviolet photoelectron spectroscopy and the optical spectrophotometer to obtain the better bi-functional device performance. With efforts, a maximum EL of 1550 cd/m^2 is achieved by optimizing the composition in the connecting layer. The forward- and reverse-biased current density-voltage characteristics in dark and under illumination are evaluated to better understand the operational mechanism of the bi-functional LE-OSCs. The finding in this work gives deep understanding of carrier transporting in tandem devices with combined PV and EL units. And the developed LE-OSCs with PV and EL units also provide a direct route to evaluate the microstructures (i.e., pinholes and defects) in organic semiconductor films.

2 Experimental

2.1 Device fabrication

Blend solutions of P3HT:$IC_{60}BA$ (1:1, in wt%) were prepared using chloroform as the solvent at a solid content of 12 mg/mL. The solutions were prepared in a nitrogen circumstance and rigorously stirred for more than 12 h at room temperature. A thin layer of poly (3,4-ethylenedioxythiophene):poly(4-styrenesulfonate) (PEDOT:PSS) and the active layer of P3HT:$IC_{60}BA$ (1:1, in wt%) were first deposited onto the patterned indium-tin-oxide (ITO) substrate sequentially by spin coating. After that, a co-evaporated interlayer of MoO_3:Al (or Ag) and a light-emitting layer CBP:$Ir(ppy)_3$ was formed, subsequently. 2,9-dimethyl-4,7-diphenylphenanthroline (BCP) was evaporated as a buffer layer. Finally, Al electrode was deposited via thermal evaporation through a shadow mask, giving an active device area of 0.04 cm^2. The whole device has a structure of ITO/PEDOT:PSS (50 nm)/P3HT:$IC_{60}BA$ (150 nm)/MoO_3:Al (5 nm)/CBP:$Ir(ppy)_3$ (15 nm)/BCP (10 nm)/Al (70 nm). Figure 1 shows the schematic diagram of the device structure and the molecule structure of the materials upon investigation. The interlayer MoO_3:Al was co-deposited in the volume ratio of 1:1.

2.2 Measurements and characterization

The current-voltage characteristics were measured using a semiconductor parameter analyzer (HP 4155B) under a simulated air mass (AM) 1.5G spectra illumination. EL characteristics were measured using both the semiconduc-

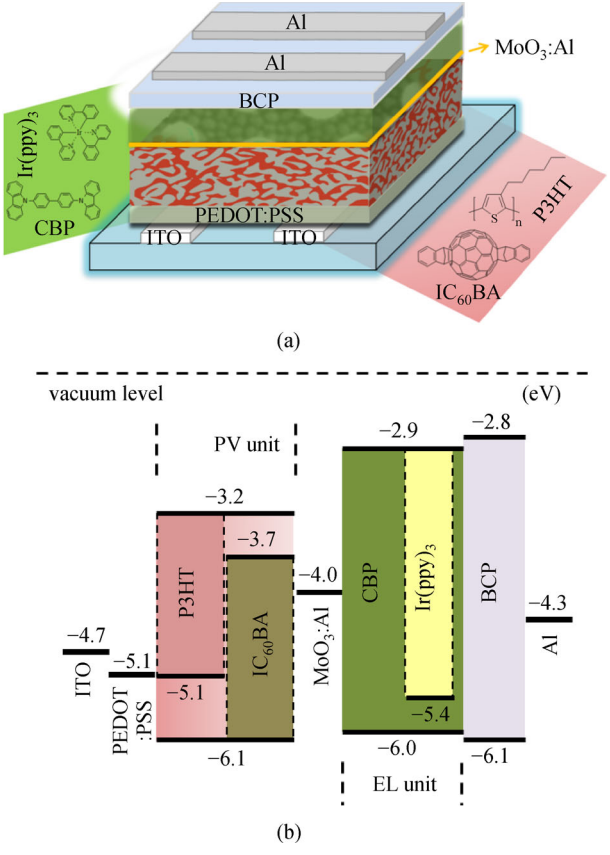

Fig. 1 (a) Schematic diagram of the light-emitting organic solar cells (LE-OSCs) and the molecule structure of materials upon investigation. (b) Energy levels of the materials in LE-OSCs

tor parameter analyzer (HP 4155B) and a luminance meter (Topcon BM-3). The transmittance spectra were collected by a spectrophotometer (Hitachi 330). The surface morphology of the blend films was evaluated using atomic force microscopy (AFM). Ultraviolet photoelectron spectroscopy (UPS) analyses were carried out with the excitation photo energy of 21.2 eV (HeI) from an unfiltered He gas discharge lamp and a hemispherical analyzer. The graphic EL imaging was taken using a digital camera (CASIO EX-F1) combined with a microfocus lens system.

3 Results and discussion

Interfacial layers are commonly used in tandem organic electronic devices by connecting two and more separated PV and/or EL units. Typical intermediate interfacial layers can be formed by conductive films [33], organic heterojunction [34], and n-doped/metal oxide junction [35] with good optical and electrical characteristic [36,37]. Among them, MoO_3 is widely used as an anode interfacial material in OLEDs and OSCs owing to its relative low evaporation temperature, non-toxicity and deep electronic states [38–40]. The work function of MoO_3 can be tuned by doping using some metal materials with lower work function. The UPS spectra of pure MoO_3, and co-evaporated MoO_3:Al are displayed in Fig. 2. The inset is the enlarged regions of the photoemission secondary-electron cutoffs. The work function of the pure MoO_3 was estimated to be 5.1 eV, which is lower than the ultra-high vacuum *in situ* value due to the effect of oxygen and moisture by air exposure. When doping by Al, a downward shift of the vacuum level was observed, corresponding to a decrease in work function with 1.0 eV for MoO_3:Al.

One requirement for the connecting layer in tandem devices is the good optical transparency which can guarantee sufficient light transmittance between the PV and/or EL units. Figure 3 shows the transmission spectra of P3HT:IC_{60}BA blend (150 nm), P3HT:IC_{60}BA (150 nm)/MoO_3:Ag (5 nm) and P3HT:IC_{60}BA (150 nm)/MoO_3:Al (5 nm). Compared to the as-coated P3HT:IC_{60}BA blending film, additional deposition of a thin MoO_3:Ag (Al) results in an upward shift of transmission spectra, which is assumed to be associated with the localized surface plasmon resonance effect of Ag and Al nanoparticles formed in MoO_3:Ag (Al) film during co-evaporation [41,42]. In addition, the transmittance of P3HT:IC_{60}BA (150 nm)/MoO_3:Al (5 nm) is slightly higher than that of P3HT:IC_{60}BA (150 nm)/MoO_3:Ag (5 nm) at 512 nm (EL peak of $Ir(ppy)_3$). It means that more light generated in the EL unit would pass through the interfacial layer if using MoO_3:Al as a connecting layer.

Figure 4 shows the typical current density – voltage ($J-V$) characteristics in tandem devices with and without interfacial layer (IL) under illumination (100 mW/cm^2). The $J-V$ characteristics of a P3HT:IC_{60}BA based OSC device (OSC only) with structure of ITO/PEDOT (50 nm)/P3HT:IC_{60}BA (150 nm)/LiF (1 nm)/Al (70 nm) is also shown for comparison. The referenced device (OSC only) shows a power conversion efficiency (PCE) of 4.45% with short-circuit current density (J_{sc}) = 10.85 mA/cm^2, open-circuit voltage (V_{oc}) = 0.76 V and fill factor (FF) = 54%. For tandem devices without any interfacial layer (W/O IL), poor PV property with J_{sc} = 0.08 mA/cm^2, V_{oc} = 0.45 V and FF = 22% is achieved. The competing EL and PV mechanisms lead to the poor device performance because the charge carrier behavior is not tuned by a suitable interfacial layer. After using MoO_3:Al as an interfacial layer, the carrier injection and transport characteristics in both PV and EL units are improved, resulting in enhanced J_{sc} (0.96 mA/cm^2), V_{oc} (0.70 V), and FF (36%), corresponding to an improved PCE of 0.24%. The detailed

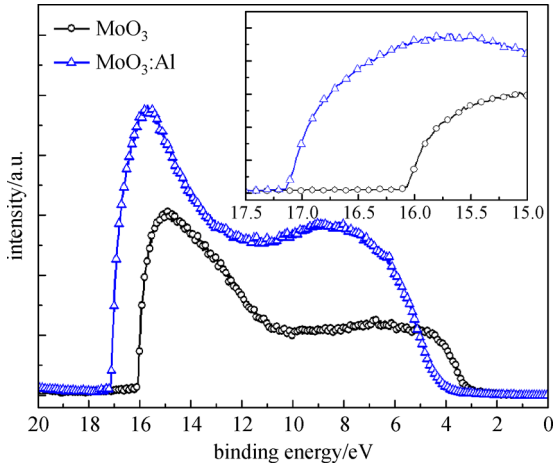

Fig. 2 Ultraviolet photoelectron spectroscopy (UPS) spectra of pure MoO_3, co-evaporated MoO_3:Al films. The inset is the enlarged regions of the photoemission secondary-electron cut-offs

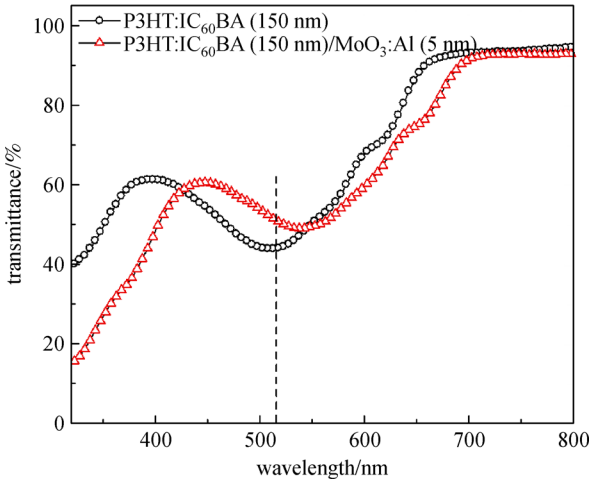

Fig. 3 Transmittance spectra of P3HT:IC_{60}BA (150 nm) and P3HT:IC_{60}BA (150 nm)/MoO_3:Al (5 nm). The dash line is a sign of EL peak of $Ir(ppy)_3$

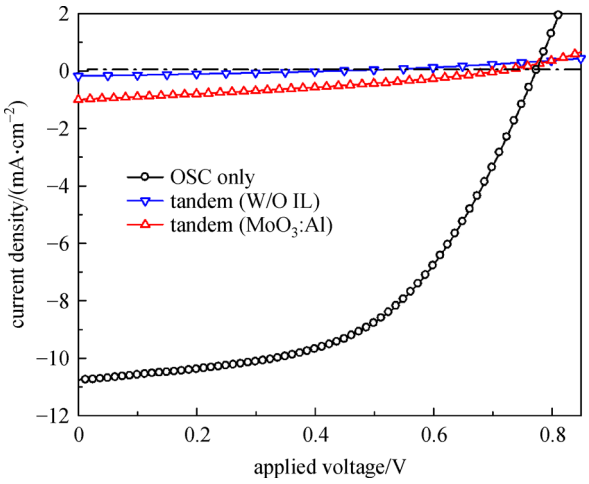

Fig. 4 Current density–voltage (J–V) characteristics in the LE-OSCs with and without (W/O) interfacial layer (IL) and the reference device (OSC only) with a structure of ITO/PEDOT (50 nm)/P3HT:$IC_{60}BA$ (150 nm)/LiF (1 nm)/Al (70 nm) under illumination (100 mW/cm^2)

PV and EL characteristics in all tandem devices are summarized in Table 1.

Figure 5 shows the EL properties for (a) $J-V$ and (b) luminance vs current density ($L-J$) characteristics, respectively, in LE-OSCs with and without interfacial layer in dark condition. The EL property of a CBP:$Ir(ppy)_3$ based OLED device (OLED only) with structure of ITO/PEDOT (50 nm)/CBP:$Ir(ppy)_3$ (80 nm)/BCP (10 nm)/Al (70 nm) is also shown for comparison. The reference device (OLED only) exhibits a turn-on voltage (V_t) of 1.6 V and a maximum luminance (L_{max}) of 40800 cd/m^2. For LE-OSC without any interfacial layer, the EL property largely deteriorates with a V_t of 4.4 V and an L_{max} of 140 cd/m^2 due to no tuneable carrier behavior by a suitable interfacial layer. The decreased device performance of EL unit was originated from the reduced electron extraction due to its direct contact with the PV unit. Since MoO_3:Al is a co-evaporation interfacial layer with bipolar carrier transporting properties, the hole can be injected into the EL unit from the PV unit. By inserting an interfacial layer of MoO_3:Al between the PV and EL units, the EL properties of LE-OSCs are remarkably improved. For example, in the case of using MoO_3:Al as an interfacial layer, V_t is lowered from 4.4 to 3.2 V, and a maximum luminance of

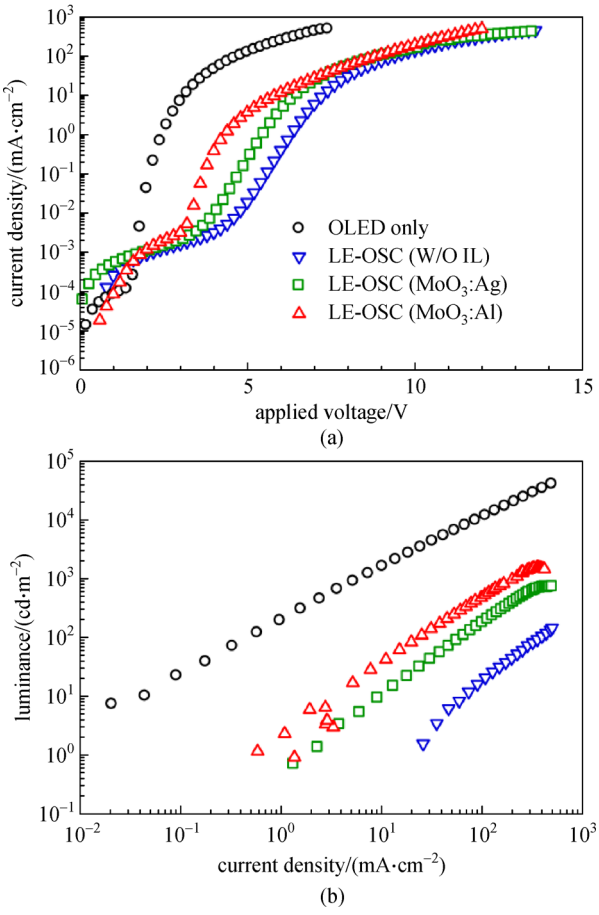

Fig. 5 EL properties for (a) current density–voltage (J–V) and (b) luminance vs current density (L–J) characteristics, respectively, in LE-OSCs with and without (W/O) interfacial layer (IL) in dark condition

1550 cd/m^2 is achieved.

Figure 6 shows the forward- and reverse-biased $J-V$ characteristics of tandem devices in dark and under illumination (100 mW/cm^2). The insets are the corresponding double-logarithmic plots. In both cases, EL emission is observed only at forward bias. And there exists no large difference on the EL properties. In addition, the contribution of light harvesting in the PV unit to the total current is observed in the low forward bias region (< 3 V) because the EL current is far larger than the photo-induced current. While, the photo-induced current is very obvious in whole reverse bias region. Particularly, a trap-assistant current

Table 1 PV and EL properties in LE-OSCs with and without (W/O) interfacial layers (IL). The performance of reference devices (OSC only and OLED only) is also shown

device	V_t/V	L^*/(cd·m^{-2})	L_{max}/(cd·m^{-2})	V_{oc}/V	J_{sc}/(mA·cm^{-2})	FF/%	PCE/%
OSC-only	–	–	–	0.76	10.85	54	4.45
OLED-only	1.6	9950	40800	–	–	–	–
tandem (W/O IL)	4.4	20	140	0.45	0.08	22	0.008
tandem (MoO_3:Al)	3.2	470	1550	0.70	0.96	36	0.24

Notes: V_t, turn-on voltage; L, luminance; *, under illumination (100 mW/cm^2); V_{oc}, open-circuit voltage; J_{sc}, short-circuit current density; FF, fill factor; PCE, power conversion efficiency

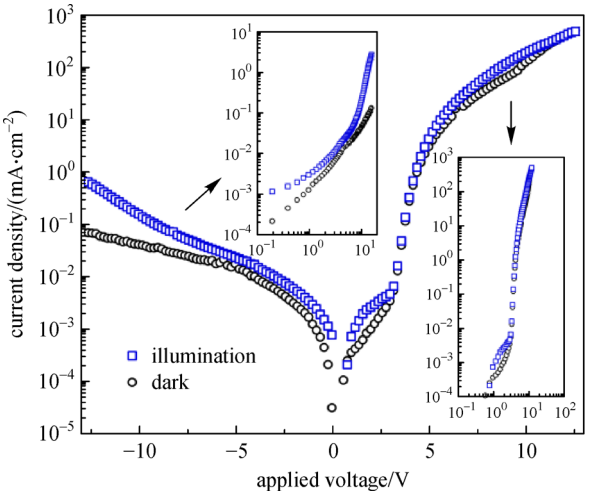

Fig. 6 Forward- and reverse-biased current density–voltage (J–V) characteristics of LE-OSCs in dark and under illumination (100 mW/cm^2). The insets are the corresponding double-logarithmic plots

appears in high reverse-bias (>10 V) from the double-logarithmic plot. As shown in Fig. 1(b), the highest occupied molecular orbital (HOMO) of $IC_{60}BA$ in the active layer of the PV unit is similar to that of CBP in the light-emitting layer of the EL unit. It is reported that the hole injection can be realized either through direct injection from the anode or subsequent transfer of holes from polymer to fullerene [29]. At the same time, the high work function of MoO_3 in the MoO_3:Al interfacial layer produces a route to the hole injection from the PV unit to the EL unit. Considering the direct electron injection through BCP and further blocking of holes by BCP, EL unit can operate effectively. Under illumination, light harvesting, exciton generation and carrier separation in the PV unit can also be carried out effectively. However, the electron extraction is largely confined by the large difference of the lowest unoccupied molecular orbital (LUMO) between $IC_{60}BA$ and CBP. The functions and charge transporting, such as charge transport, light-emission, and light harvesting in PV and EL devices, are very different. And the light production and current generation in them are a competing phenomenon due to their reverse generation mechanism. We developed MoO_3:Al connecting layer enables the PV and EL tandem device operate very well. The current density–voltage characteristics analysis gave a further understanding of carrier transporting in tandem devices with combined PV and EL units.

As an application, the EL imaging in the tandem device is used as a background light source for observing the film conditions of P3HT:$IC_{60}BA$ blending films. Figure 7 shows the photograph of EL imaging (2 mm × 2 mm) of (a) pinholes, (b) film uniformity and (c) strip lines of P3HT:$IC_{60}BA$ blending films in different samples. The

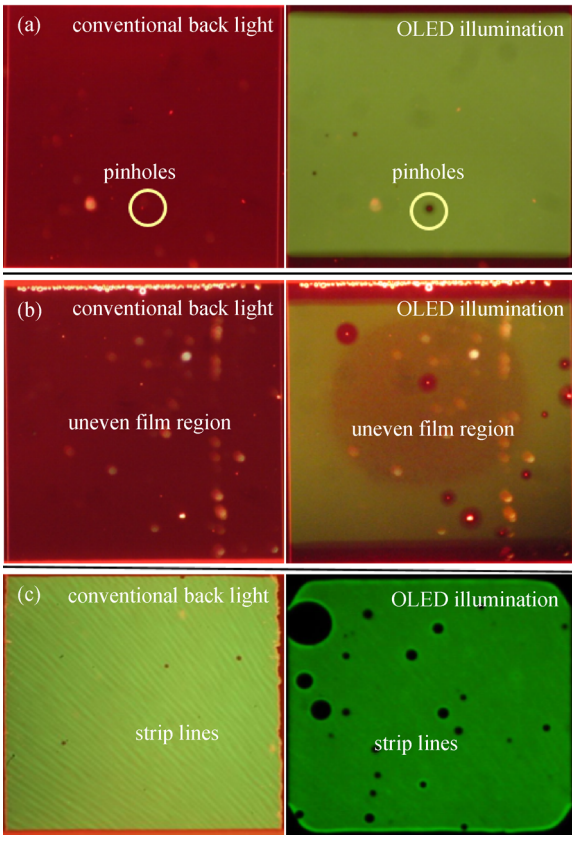

Fig. 7 Photograph and EL imaging (2 mm × 2 mm) of (a) pinholes, (b) film uniformity and (c) strip lines of P3HT:$IC_{60}BA$ blending films in different samples observed by conventional back light and OLED imaging

dusts, the hot spots, the defects, and even the polymer aggregation in P3HT:$IC_{60}BA$ bulk film can be seen clearly by an optical microscope with black light illumination. Whereas, as shown in Fig. 7(a), the dusts, the defects and the pinholes can be distinguished clearly by using the OLED as a back illumination. Interestingly, an uneven film region (1.5 mm × 1.0 mm) of P3HT:$IC_{60}BA$ bulk film, which could not be reflected in the optical microscopic image, is observed obviously by using an OLED as the back light source as shown in Fig. 7(b). Generally, the polymer:fullerene film in practical application is very thin (~100 nm), uneven film region with large area is not effectively reflected by a point light source based technique. In present case, OLED is an innate surface-emitting light source. In addition, the EL layer (OLED back light source) directly contacted with the P3HT:$IC_{60}BA$ bulk film. The film quality especially the film uniformity of P3HT:$IC_{60}BA$ blends can be reflected easily. Actually, the cell degradation is seriously associated with the film uniformity of the active layer besides the film defects. The uneven region of the active layer will be gradually broken from the center during the degradation process. We attributed it to the poor uniformity of the

P3HT:$IC_{60}BA$ blending films. In addition, the strip lines caused during the spin-coating process can also be evaluated effectively as shown in Fig. 7(c). In addition, the dark spots formed during the device degradation due to the incomplete encapsulation, were also clearly reflected from the right image of Fig. 7(c) when using OLED as the back light. In a word, direct evaluation of active film quality in OSCs can be easily realized by using the OLED as a background light source.

Actually, for most organic semiconductor films, the photo-oxidation due to the molecular oxygen and water will disrupt the delicate electrochemical processes, which mainly determines the key parameters and the device stability. Although the trapped charge carriers do not directly participate in the charge transport in the organic films, they still strongly affect the charge carrier behavior by their columbic forces. Therefore, the evaluation of film quality such as the trap states and the defect conditions in the active layers are very important for deeply understanding the mechanism of the cell degradation with a final goal of good cell stability. The EL imaging in our developed LE-OSCs can evaluate the film quality, such as film defect, film uniformity and the film degradation directly.

4 Conclusions

In conclusion, we have fabricated a LE-OSCs by connecting a P3HT:$IC_{60}BA$ based PV unit and a CBP:$Ir(ppy)_3$ baded EL unit using a MoO_3:Al interfacial layer. The forward- and reverse-biased $J-V$ characteristics in dark and illumination conditions are investigated to better understand the operational mechanism of the LE-OSCs. A maximum luminance of 1550 cd/m^2 under forward bias and a power conversion efficiency of 0.24% under illumination (100 mW/cm^2) are achieved by optimizing the work function and the optical property of the MoO_3:Al interfacial layer. In addition, direct observation of film condition in P3HT:$IC_{60}BA$ blends by using the EL imaging as a background light source. Since the advantages of self-emitting, surface-emitting for OLEDs, the film quality especially the uniformity of P3HT:$IC_{60}BA$ blending films was evaluated using the OLED as a background light source by operating the tandem devices under a bias mode. EL imaging in the LE-OSCs we proposed is expected to evaluate the OSC stability based on the analysis of film quality such as film defect, film uniformity and the film degradation.

Acknowledgements The authors acknowledge financial support from the National Natural Science Foundation of China (Grant No. 61674109), Jiangsu Province College Student Innovation and Entrepreneurship Training Program (No. 202010285087Y), and the Natural Science Foundation of the Jiangsu Higher Education Institutions of China (No. 19KJD510006). This project is also funded by the Collaborative Innovation Center of Suzhou Nano Science and Technology, and by the Priority Academic Program Development of Jiangsu Higher Education Institutions (PAPD).

References

1. Green M A, Hishikawa Y, Dunlop E D, Levi D H, Hohl-Ebinger J, Yoshita M, Ho-Baillie A W Y. Solar cell efficiency tables. Progress in Photovoltaics: Research and Applications, 2019, 27(1): 3–12
2. Jørgensen M, Norrman K, Gevorgyan S A, Tromholt T, Andreasen B, Krebs F C. Stability of polymer solar cells. Advanced Materials, 2012, 24(5): 580–612
3. Kumar P, Chand S. Recent progress and future aspects of organic solar cells. Progress in Photovoltaics: Research and Applications, 2012, 20(4): 377–415
4. Kroon R, Lenes M, Hummelen J, Blom P, Boer B. Small bandgap polymers for organic solar cells (polymer material development in the last 5 years). Polymer Reviews (Philadelphia, Pa.), 2008, 48(3): 531–582
5. Dou L, You J, Yang J, Chen C, He Y, Murase S, Moriarty T, Emery K, Li G, Yang Y. Tandem polymer solar cells featuring a spectrally matched low-bandgap polymer. Nature Photonics, 2012, 6(3): 180–185
6. Honda S, Nogami T, Ohkita H, Benten H, Ito S. Improvement of the light-harvesting efficiency in polymer/fullerene bulk heterojunction solar cells by interfacial dye modification. ACS Applied Materials & Interfaces, 2009, 1(4): 804–810
7. Suresh P, Balraju P, Sharma G D, Mikroyannidis J A, Stylianakis M M. Effect of the incorporation of a low-band-gap small molecule in a conjugated vinylene copolymer: PCBM blend for organic photovoltaic devices. ACS Applied Materials & Interfaces, 2009, 1(7): 1370–1374
8. Reese M O, Nardes A, Rupert M B L, Larsen R E, Olson D C, Lloyd M T, Shaheen S E, Ginley D S, Rumbles G, Kopidakis N. Photoinduced degradation of polymer and polymer–fullerene active layers: experiment and theory. Advanced Functional Materials, 2010, 20(20): 3476–3483
9. Abad J, Urbina A, Colchero J. Influence of UV radiation and ozone exposure on the electro-optical properties and nanoscale structure of P3OT films. Organic Electronics, 2011, 12(8): 1389–1398
10. Krebs F C, Tromholt T, Jørgensen M. Upscaling of polymer solar cell fabrication using full roll-to-roll processing. Nanoscale, 2010, 2(6): 873–886
11. Schäfer S, Petersen A, Wagner T, Kniprath R, Lingenfelser D, Zen A, Kirchartz T, Zimmermann B, Würfel U, Feng X, Mayer T. Influence of the indium tin oxide/organic interface on open-circuit voltage, recombination, and cell degradation in organic small-molecule solar cells. Physical Review B, 2011, 83(16): 165311
12. Yu G, Gao J, Hummelen J, Wudl F, Heeger A. Polymer photovoltaic cells: enhanced efficiencies via a network of internal donor-acceptor heterojunctions. Science, 1995, 270(5243): 1789–1791
13. Wang M, Tang Q, An J, Xie F, Chen J, Zheng S, Wong K, Miao Q, Xu J. Performance and stability improvement of P3HT:PCBM-based solar cells by thermally evaporated chromium oxide (CrO_x) interfacial layer. ACS Applied Materials & Interfaces, 2010, 2(10): 2699–2702

14. Hains A W, Liu J, Martinson A B F, Irwin M D, Marks T J. Anode interfacial tuning via electron-blocking/hole-transport layers and indium tin oxide surface treatment in bulk-heterojunction organic photovoltaic cells. Advanced Functional Materials, 2010, 20(4): 595–606
15. Xu M, Cui L, Zhu X, Gao C, Shi X, Jin Z, Wang Z, Liao L. Aqueous solution-processed MoO_3 as an effective interfacial layer in polymer/fullerene based organic solar cells. Organic Electronics, 2013, 14(2): 657–664
16. Xu Z, Chen L, Yang G, Huang C, Hou J, Wu Y, Li G, Hsu C, Yang Y. Vertical phase separation in poly(3-hexylthiophene): fullerene derivative blends and its advantage for inverted structure solar cells. Advanced Functional Materials, 2009, 19(8): 1227–1234
17. Norrman K, Gevorgyan S A, Krebs F C. Water-induced degradation of polymer solar cells studied by $H_2{}^{18}O$ labeling. ACS Applied Materials & Interfaces, 2009, 1(1): 102–112
18. Lira-Cantu M, Norrman K, Andreasen J, Krebs F. Oxygen release and exchange in niobium oxide MEHPPV hybrid solar cells. Chemistry of Materials, 2006, 18(24): 5684–5690
19. Alstrup J, Jørgensen M, Medford A J, Krebs F C. Ultra fast and parsimonious materials screening for polymer solar cells using differentially pumped slot-die coating. ACS Applied Materials & Interfaces, 2010, 2(10): 2819–2827
20. von Malm N, Steiger J, Schmechel R, von Seggern H. Trap engineering in organic hole transport materials. Journal of Applied Physics, 2001, 89(10): 5559–5563
21. Schmechel R, von Seggern H. Electronic traps in organic transport layers. Physica Status Solidi, 2004, 201(6): 1215–1235
22. Graupner W, Leditzky G, Leising G, Scherf U. Shallow and deep traps in conjugated polymers of high intrachain order. Physical Review B, 1996, 54(11): 7610–7613
23. Okachi T, Nagase T, Kobayashi T, Naito H. Determination of localized-state distributions in organic light-emitting diodes by impedance spectroscopy. Applied Physics Letters, 2009, 94(4): 043301
24. Harada K, Riede M, Leo K, Hild O R, Elliott C M. Pentacene homojunctions: electron and hole transport properties and related photovoltaic responses. Physical Review B, 2008, 77(19): 195212
25. Lou Y, Xu M, Zhang L, Wang Z, Naka S, Okada H, Liao L. Origin of enhanced electrical and conducting properties in pentacene films doped by molybdenum trioxide. Organic Electronics, 2013, 14(10): 2698–2704
26. Fuyuki T, Kondo H, Yamazaki T, Takahashi Y, Uraoka Y. Photographic surveying of minority carrier diffusion length in polycrystalline silicon solar cells by electroluminescence. Applied Physics Letters, 2005, 86(26): 262108
27. Würfel P, Trupke T, Puzzer T, Schäffer E, Warta W, Glunz S. Diffusion lengths of silicon solar cells from luminescence images. Journal of Applied Physics, 2007, 101(12): 123110
28. Breitenstein O, Bauer J, Trupke T, Bardos R. On the detection of shunts in silicon solar cells by photo- and electroluminescence imaging. Progress in Photovoltaics: Research and Applications, 2008, 16(4): 325–330
29. Rau U. Reciprocity relation between photovoltaic quantum efficiency and electroluminescent emission of solar cells. Physical Review B, 2007, 76(8): 085303
30. Cravino A, Leriche P, Aleveque O, Roquet S, Roncali J. Light-emitting organic solar cells based on a 3D conjugated system with internal charge transfer. Advanced Materials, 2006, 18(22): 3033–3037
31. Hoyer U, Wagner M, Swonke T, Bachmann J, Auer R, Osvet A, Brabec C. Electroluminescence imaging of organic photovoltaic modules. Applied Physics Letters, 2010, 97(23): 233303
32. Tvingstedt K, Vandewal K, Gadisa A, Zhang F, Manca J, Inganäs O. Electroluminescence from charge transfer states in polymer solar cells. Journal of the American Chemical Society, 2009, 131(33): 11819–11824
33. Sun J, Zhu X, Peng H, Wong M, Kwok H. Effective intermediate layers for highly efficient stacked organic light-emitting devices. Applied Physics Letters, 2005, 87(9): 093504
34. Liao L, Klubek K P, Tang C W. High-efficiency tandem organic light-emitting diodes. Applied Physics Letters, 2004, 84(2): 167–169
35. Kanno H, Holmes R, Sun Y, Kena-Cohen S, Forrest S. White stacked electrophosphorescent organic light-emitting devices employing MoO_3 as a charge-generation layer. Advanced Materials, 2006, 18(3): 339–342
36. Sun J, Zhu X, Peng H, Wong M, Kwok H. Bright and efficient white stacked organic light-emitting diodes. Organic Electronics, 2007, 8 (4): 305–310
37. Hamwi S, Meyer J, Kröger M, Winkler T, Witte M, Riedl T, Kahn A, Kowalsky W. The role of transition metal oxides in charge-generation layers for stacked organic light-emitting diodes. Advanced Functional Materials, 2010, 20(11): 1762–1766
38. Tokito S, Noda K, Taga Y. Metal oxides as a hole-injecting layer for an organic electroluminescent device. Journal of Physics D, Applied Physics, 1996, 29(11): 2750–2753
39. Murase S, Yang Y. Solution processed MoO_3 interfacial layer for organic photovoltaics prepared by a facile synthesis method. Advanced Materials, 2012, 24(18): 2459–2462
40. Lou Y, Xu M, Wang Z, Naka S, Okada H, Liao L. Dual roles of MoO_3-doped pentacene thin films as hole-extraction and multi-charge-separation functions in pentacene/C_{60} heterojunction organic solar cells. Applied Physics Letters, 2013, 102(11): 113305
41. Morfa A, Rowlen K, Reilly T, Romero M, Lagemaat J. Plasmon-enhanced solar energy conversion in organic bulk heterojunction photovoltaics. Applied Physics Letters, 2008, 92(1): 013504
42. Xu M F, Zhu X Z, Shi X B, Liang J, Jin Y, Wang Z K, Liao L S. Plasmon resonance enhanced optical absorption in inverted polymer/fullerene solar cells with metal nanoparticle-doped solution-processable TiO_2 layer. ACS Applied Materials & Interfaces, 2013, 5(8): 2935–2942

Xinran Li is an undergraduate student in Department of New Energy Materials and Devices, Soochow University, China. From 2019, She joined Dr. Yanhui Lou's group for the training program of innovation and entrepreneurship for undergraduates. Her research interest is thin film solar cells.

Yanhui Lou received her Ph.D. degree in Nano and Novel Matter Science from University of Toyama, Japan, in 2012. After working at University of Toyama as a JSPS research fellow from 2012 to 2014, she joined Soochow Institute for Energy and Materials Innovations, Soochow University, China, as an associate professor. Her main research interest is focus on organic and inorganic/organic hybrid materials for application in solar cells.

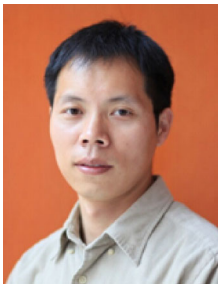

Zhaokui Wang received his Ph.D. degree in Nano and Novel Matter Science from University of Toyama, Japan, in 2011. After working at University of Toyama as a JSPS research fellow from 2011 to 2013, he joined Institute of Functional Nano & Soft Materials (FUNSOM), Soochow University, China, as an associate professor. Since 2017, he has been a full professor at Soochow University, China. His main research interests lie in organic and inorganic/organic hybrid materials and devices, focusing on solar cells and organic light-emitting diodes (OLEDs).